Kinetics of γ' Precipitation and Its Influence on Fatigue Crack Growth Behavior of a New Single-Crystal Nickel-Based Superalloy (CMSX-4G) at Room Temperature

A. Sengupta and S.K. Putatunda

An investigation was carried out to determine the growth kinetics of γ' precipitates in a newly developed single-crystal nickel-base superalloy containing rhenium (CMSX-4G). The investigation also examined the influence of γ' precipitates (size and distribution) on fatigue crack growth behavior of the material in a room-temperature ambient atmosphere. The influence of load ratio on fatigue threshold of the material and crack growth mechanisms in fatigue was also studied. Compact tension specimens were prepared from a single-crystal nickel-base superalloy, CMSX-4G, with the ⟨001⟩ crystallographic direction. These specimens were given two different heat treatments to produce two different γ' size precipitates. Fatigue crack growth behavior of these materials was studied at three different load ratios (R = 0.10, 0.50, and 0.90) in room-temperature ambient atmosphere. The results of the present investigation demonstrate that rhenium additions in CMSX-4G substantially lowers the γ' coarsening kinetics of this alloy. The smaller γ' precipitate size was found to be beneficial for fatigue resistance and has resulted in a higher fatigue threshold and lower fatigue crack growth rate in the threshold region. The fatigue threshold was found to decrease with an increase in load ratio. The crack growth mechanism in the threshold region was found to occur by a combination of microvoid coalescence and striations.

Keywords
crack growth, fatigue, kinetics, nickel alloys, performance test: fatigue, precipitation, superalloys

1. Introduction

SUPERALLOYSare high-temperature heat-resistant materials capable of retaining very high strengths at elevated temperatures. These complex alloys have good corrosion and oxidation resistance and superior resistance to creep and stress-rupture at high temperatures. In general, there are three basic groups[1] of superalloys: nickel-base, iron-base, and cobalt-base.

Because of their superior strength at elevated temperatures[2,3] compared to cobalt- and iron-base superalloys, the most widely used superalloys in high-temperature applications are nickel-base. These materials are used extensively in many high-temperature applications such as aircraft, marine, and industrial gas turbines, space vehicles, rocket engines, nuclear reactors, etc. Their applicability is based on the presence of chromium, which imparts primarily oxidation and high-temperature corrosion resistance, and other alloying elements such as titanium, aluminum, cobalt, tungsten, etc., which impart high-temperature strength and creep resistance.

A. Sengupta, Graduate Research Assistant, Department of Chemical and Materials Science and Engineering, Wayne State University, Detroit, Michigan, and **S.K. Putatunda,** Associate Professor, Department of Chemical and Materials Science and Engineering, Wayne State University, Detroit, Michigan.

The microstructure of the nickel-base superalloys consists of several phases,[4-6] such as the γ phase, which is a continuous matrix of face-centered cubic (fcc) structure; the γ' phase, which is the major precipitation phase; and frequently carbides. These carbides are basically of two types: $M_{23}C_6$[7] and MC[7], where M stands for any metal.

Most of the nickel-base superalloys depend on chromium additions for their oxidation and hot corrosion resistance. They depend on aluminum and titanium for strength. These elements allow the precipitation of an ordered compound based on the formula Ni_3(Al-Ti). This phase is called γ' phase to distinguish it from the fcc matrix γ phase. The γ' phase has an ordered $L1_2$ type of structure. It has a unique feature in that its strength increases[8] at higher temperatures. The γ' phase is coherent with its matrix. The mechanical properties of these superalloys depend on such factors as the amount of γ' phase, its morphology, and the elastic strain induced by it when it precipitates because of the lattice mismatch between γ' precipitate and the γ matrix.

Single-crystal nickel-base superalloys have the highest temperature capability[9,10] and the best combination of elevated temperature properties of any structural material. The superiority of single crystals over polycrystalline superalloys is due to their very high creep resistance because of the absence of grain boundaries and their higher incipient melting temperature above the γ' solvus temperature. This allows the γ' microstructure to be refined through a solution treatment for increased creep resistance of the alloy.

The nickel-base superalloy CMSX-4G is a newly developed material and is cast in the form of a single crystal. This alloy is strengthened by the solid solution strengthening effects of tungsten, tantalum, and rhenium. The presence of rhenium pro-

Table 1 Chemical Composition of CMSX-4G

Composition	wt%
Chromium	6.0
Cobalt	10.0
Molybdenum	0.6
Tungsten	6.0
Tantalum	6.0
Rhenium	3.0
Aluminum	6.0
Titanium	1.0
Hafnium	0.1
Nickel	bal

Table 2 Heat Treatment Procedures for Kinetics Study

1. As cast bar: Solution treatment at 2330 °F for 2 h, at 2350 °F for 2 h, at 2365 °F for 3 h, at 2380 °F for 3 h, at 2395 °F for 2 h, at 2400 °F for 2 h, at 2410 °F for 2 h and finally air cooled
   Resultant γ' size: $r_0 = 0.0$ μm
2. After above solution treatments: High-temperature aging at 1975 °F for 4 h, air cooled, final aging at 1600 °F for 20 h, then air cooled
   Resultant γ' size: $r_1 = 0.3$ μm
3. Solution treated alloy (after Treatment 1) at 2354 °F for 4 h, air cooled, solution treatment at 2354 °F for 2 h, water quench, then high-temperature aging at 1975 °F for 4 h, air cooled, final aging at 1600 °F for 59 h
   Resultant γ' size: $r_2 = 0.54$ μm
4. Solution treated alloy (after Step 1): High-temperature aging at 1975 °F 4 h, air cooled, then final aging at 1600 °F for 150 h
   Resultant γ' size: $r_3 = 0.8$ μm
5. Solution treated alloy (after heat treatment 1): High-temperature aging at 1975 °F for 4 h, air cooled, then final aging at 1600 °F for 1000 h
   γ' size: $r_4 = 0.9$ μm

vides increased creep resistance in this alloy at elevated temperatures. This alloy features a 64 °F[11,12] advantage over the first-generation single-crystal alloys such as CMSX-2 and CMSX-3 in stress-rupture temperature capability at 1800 °F.[12] It contains a reduced level of chromium, and thus, the solubility of titanium and aluminum is increased at higher temperatures. At the same time, any decrease in the oxidation resistance due to a reduced level of chromium is offset by the increased aluminum content of the alloy.

The presence of rhenium can[13] influence the growth kinetics of γ' precipitates in nickel-base superalloys. However, the growth kinetics of γ' in CMSX-4G is not clearly known or established. Therefore, this aspect needs to be examined in detail. Moreover, the size, shape, and distribution of γ' can significantly influence the fatigue crack growth rate and fatigue threshold of the material.

The primary objective of the present investigation was to determine the growth kinetics of γ' precipitates in the single-crystal nickel-base superalloy CMSX-4G in presence of rhenium. The secondary objective of this investigation was to examine the influence of γ' precipitates (size and distribution) on fatigue crack growth rate and fatigue threshold of the material in room-temperature ambient atmosphere. The fatigue crack growth data of the material at elevated temperature will be reported in a later publication.

Table 3 Heat Treatment Procedures for Compact Tension Specimens

Heat treatment condition A: As-received bar was solution heated at 2330 °F for 2 h, at 2350 °F for 2 h, at 2365 °F for 3 h, at 2380 °F for 3 h, at 2395 °F for 2 h, at 2400 °F for 2 h, at 2405 °F for 2 h, at 2410 °F for 2 h, and finally air cooled
High-temperature aging at 1975 °F for 4 h, then air cooled, finally aged at 1600 °F for 20 h, and air cooled
γ' size: 0.3 μm
Heat treatment condition B: Two-step aging (after heat treatment condition A) aged at 2085 °F for 6 h, air cooled, then finally aged at 1600 °F for 100 h and then air cooled
γ' size: 0.5 μm

2. Experimental Procedure

2.1 *Material*

The material used in this investigation was the single-crystal nickel-base superalloy CMSX-4G. The chemical composition of the material is given in Table 1. The master alloy was vacuum cast, and single crystals were grown by the modified Bridgman technique. Crystals were grown parallel to the ⟨001⟩ direction. Their orientation was verified by the back reflection Laue technique. The crystals were grown such that ⟨100⟩ planes were parallel to the specimen faces.

2.2 *Heat Treatments*

For kinetics study, metallographic specimens were cut in the size of 0.25 in. round and 0.1 in. thickness from single-crystal alloy in the ⟨001⟩ orientation. These specimens were given a series of sequential isothermal heat treatments followed by aging at several temperatures for a predetermined time. The details of these heat treatments are given in Table 2.

Sections of the heat treated samples were examined by scanning electron microscopy (SEM). The precipitates examined in this study were cuboidal in nature. Precipitate size determination was made from the micrographs such that cube edge lengths in two directions were measured for at least 200 precipitates. Precipitate dimensions were taken to be half of the cube edge of γ' precipitates. The γ' size measurements were done on optically polished specimens after etching with kailing reagent (25 g copper chloride, 55 cm^3 ethanol, and 50 cm^3 HCl). Statistical analysis was carried out to determine the size distribution of γ' precipitates. Four different size γ' precipitates were produced as a result of the heat treatment processes, and these are shown in Fig. 1(a) through (d). The average size of γ' precipitates as a result of these heat treatments also are listed in Table 2.

2.3 *Fatigue Testing*

For fatigue threshold testing, 2(T) compact tension specimens were prepared from single-crystal CMSX-4G material with ⟨001⟩ tensile orientation in accordance with ASTM Standard E-647.[14] The width of the specimens was kept at 50.8 mm and thickness about 12 mm. The aspect ratio was kept at $a/W = 0.40$. Fabrication of specimens from test blocks was done by the electric discharge machine (EDM) procedure. A schematic

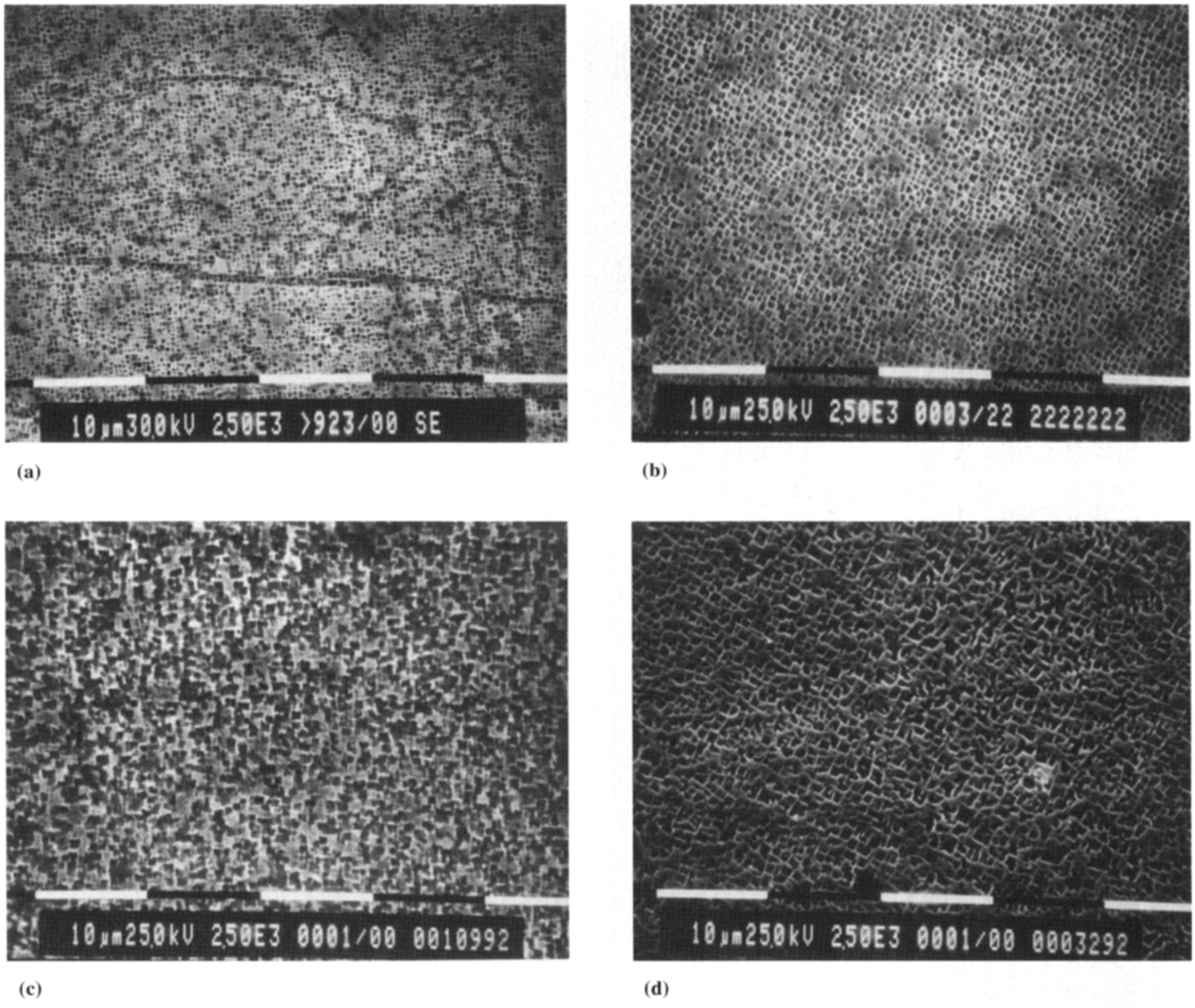

Fig. 1 Microstructure of the material indicating different γ' precipitates. **(a)** Microstructure after heat treatment 1 (Table 2). Resultant γ' size: 0.3 µm (magnification, 2500×). **(b)** Microstructure after heat treatment 2 (Table 2). Resultant γ' size: 0.54 µm (magnification, 2500×). **(c)** Microstructure after heat treatment 3 (Table 2). Resultant γ' size: 0.8 µm (magnification, 2500×). **(d)** Microstructure after heat treatment 4 (Table 2). Resultant γ' size: 0.9 µm (magnification, 2500×).

of the compact tension specimens used in this study is shown in Fig. 2. The loading direction was ⟨001⟩.

After fabrication, the compact tension specimens were given two different heat treatments to produce two different γ' precipitate sizes. These two heat treated conditions are identified as condition A and B, respectively. The microstructures of the heat treated compact tension specimens are shown in Fig. 3(a) and 3(b). The details of the above heat treatments are given in Table 3.

After heat treatment, the compact tension specimens were ground on both surfaces and then polished with 600-grit emery paper to a mirror-finished surface. Finally, they were cleaned and degreased in acetone. These procedures were helpful in locating the crack tip during fatigue testing.

The specimens were initially precracked in fatigue at a ΔK level of $\Delta K \cong 20$ MPa $\sqrt{\text{m}}$ to produce a 2-mm long sharp crack front in accordance with ASTM Standard E-647.[14] After precracking, fatigue testing was carried out using a servohydraulic MTS test machine in the load control mode. The crack lengths were monitored with the help of an optical traveling microscope. The crack lengths and number of cycles were continuously recorded. All tests were carried out in room-temperature ambient atmosphere in tension-tension mode. A constant-amplitude sinusoidal waveform was applied, and tests were carried out at three different load ratios ($R = 0.1$, 0.5, and 0.9).

The fatigue threshold was determined using the load-shedding technique per ASTM Standard E-647.[14] For this, the load values were slowly decreased, and crack growth rates

were continuously recorded. This load reduction at any ΔK level was done up to a maximum of 5% and only after the crack had grown by at least 2 mm at any ΔK level. In this manner, any retardation effect due to prior overload was avoided. The crack growth rate (da/dN) and ΔK was plotted in terms of log da/dN versus log ΔK, and the threshold was identified graphically from this plot per ASTM Standard E-647.[14] The threshold was identified as the ΔK level at which the crack growth rate was on the order of 10^{-10} m/cycle. Three specimens from each heat treated condition were tested at each load ratios (R = 0.10, 0.5, and 0.90), and the average values from these three specimens were taken as representative of crack growth rate data and fatigue threshold.

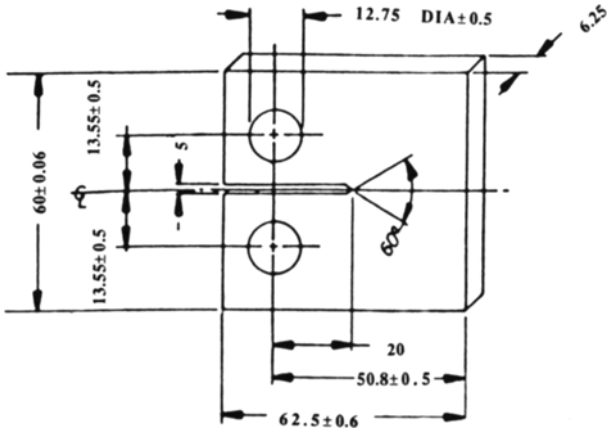

Fig. 2 Compact tension specimen, full scale. All dimensions in millimeters.

3. Results and Discussions

3.1 *Coarsening Kinetics of* γ'

As mentioned earlier, Fig. 1(a) through (d) and Table 2 show the γ' precipitate size. The precipitates were cuboidal in shape, and the size of these precipitates increases with an increase in aging time at a particular temperature. With an increase in aging time, precipitate coalescence has been observed as a result of loss of coherency between precipitates and matrix at longer aging periods. The coarsening of the γ' precipitates in nickel-aluminum binary alloys has been shown to obey theoretical predictions of known theories.[15] Lifshitz and Slyozov[16] and later Wagner[17] proposed that the average particle radius increases linearly with time and the governing equation is given by:

$$r^n - r_o^n = Kt \quad [1]$$

where r is the average radius of the particle at any given instant; r_o is the initial particle radius; and K is rate constant, given by:

$$K = \frac{8DgCV^2_m}{9RT} \quad [2]$$

where D is the diffusion coefficient; g is the interfacial free energy for precipitates/matrix interface; t is aging time; C is the equilibrium molar concentration of solute in matrix; R is the gas constant; T is temperature; and V_m is the molar volume of precipitates.

The above theory is known as the LSW theory for coarsening of γ' and predicts a value of n = 3 for a lattice diffusion-controlled process. From the experimentally determined values of the size of the γ' precipitates, the mean values r of these γ' precipitates were calculated for each distribution. To determine the best fitting values of the constants n and K in Eq 1, a least-

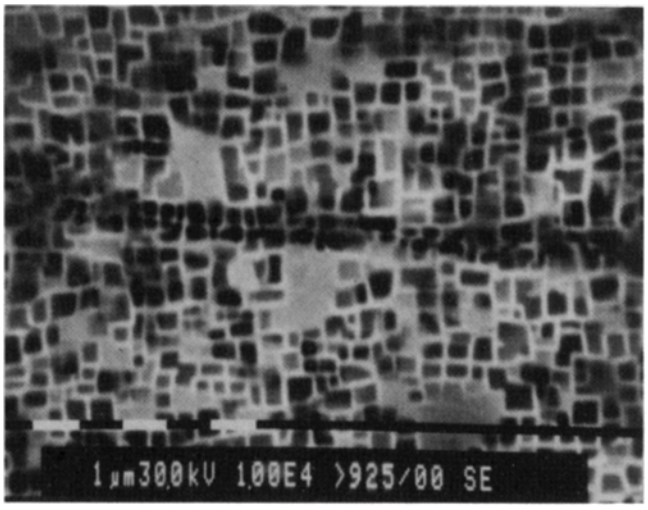

(a)

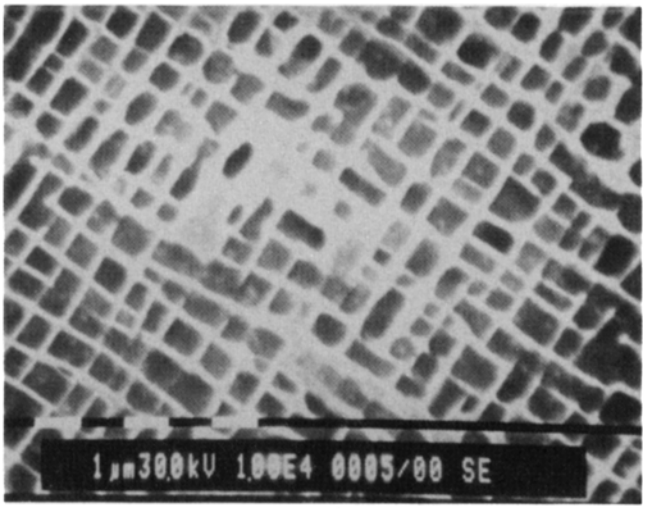

(b)

Fig. 3 Microstructure of fatigue samples. (**a**) Heat treated condition A. Resultant γ' size: 0.3 μm (magnification, 10,000×). (**b**) Heat treated condition B. Resultant γ' size: 0.5 μm (magnification, 10,000×).

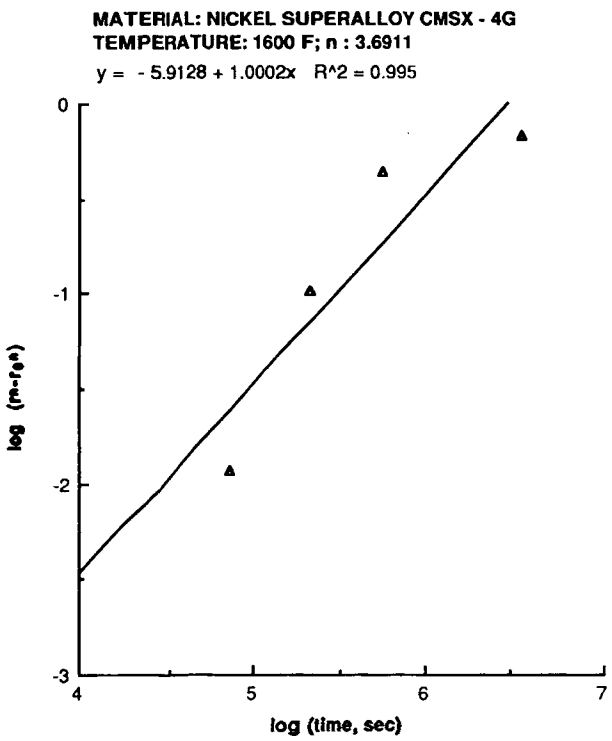

Fig. 4 Plot of log $(r^n - r_o^n)$ versus time t, using best-fit values of n.

square technique was used. A logarithmic form of Eq 1 was taken such that:

$$\log (r^n - r^n{}_o) = \log K + \log t$$

The values of n and K were then calculated using an iterative computer procedure such that the function

$$\sum_{i=1}^{w} \log [r^n - r_o^n] - [\log K - \log t]^2$$

was minimized with respect to n and K. Here, w stands for number of data points recorded for each temperature. These values were then plotted in a log-log scale in Fig. 4. The best fit straight line gives a value of $n = 3.6911$, as shown in Fig. 4.

This value of n is different (3.691) from the theoretically predicted value of $n = 3$ for lattice diffusion-controlled coarsening process,[15-17] as discussed above. Some earlier workers[13] also have found similar values for the exponent n in a rhenium-containing experimental alloy. Thus, the present test results indicate that growth kinetics of γ' in this alloy do not obey the cubic growth law and as such is not a purely lattice diffusion-controlled process. An exponent of $n = 4$ or 5 is predicted when diffusion along grain boundaries or subgrain boundaries[18] are the rate-controlling processes for Oswald ripening. However, these models are inapplicable in this alloy because of the single-crystal nature of the present alloy (no grain boundaries), and moreover, this alloy had a very low grown-in dislocation density, which precludes any significant diffusion along the subgrain boundaries.

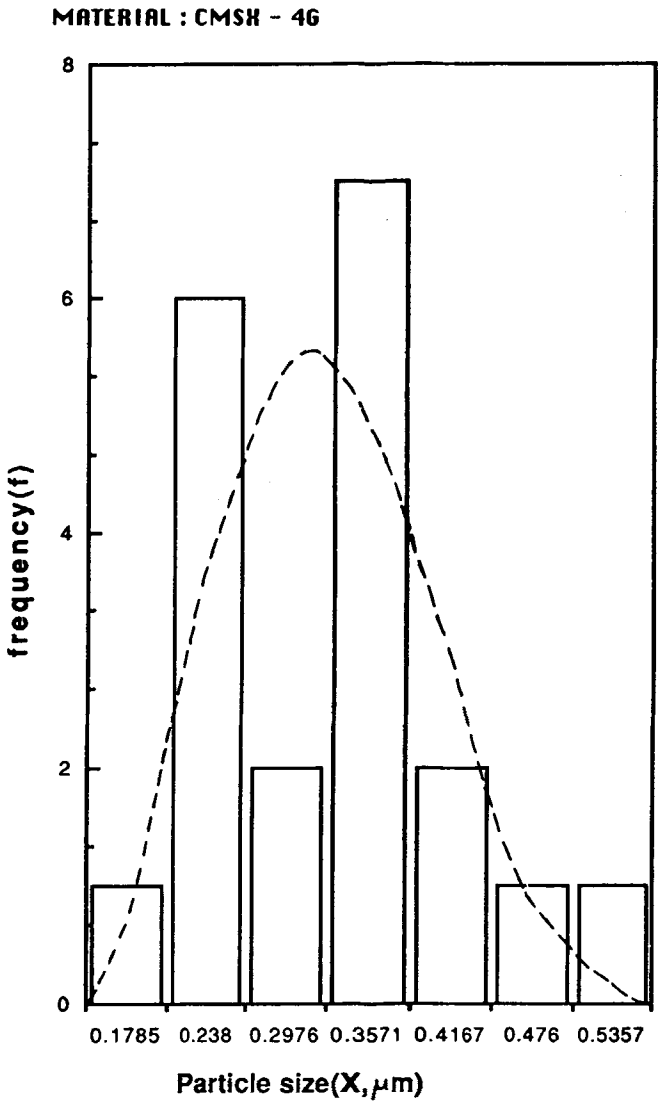

Fig. 5 Precipitate size distribution for heat treatment 1 (Table 2).

This apparent discrepancy in the value of exponent n (other than 3 as observed in the present study) is probably related to the large volume fraction of γ' as observed in this alloy. Volume fraction of γ' in this alloy was more than 70%, as evident from our micrographs. Ardell[19] and McLean[20] have shown that the LSW theory can adequately characterize the coarsening kinetics of γ' precipitates in nickel-aluminum binary alloys where the volume fraction of γ' is relatively low and the volume fraction of γ' has negligible influence on the rate constant K. However, if the volume fraction of γ' is large as in the present alloy (over 70%), this can significantly influence[20] the rate constant K and could possibly have an influence on the exponent n. Furthermore, if different mechanisms of coarsening occur concurrently then that can influence the exponent n.[18] Further studies are necessary to resolve this issue.

The activation energy for coarsening in CMSX-4G was calculated from Eq 2. Our preliminary study shows that this vol-

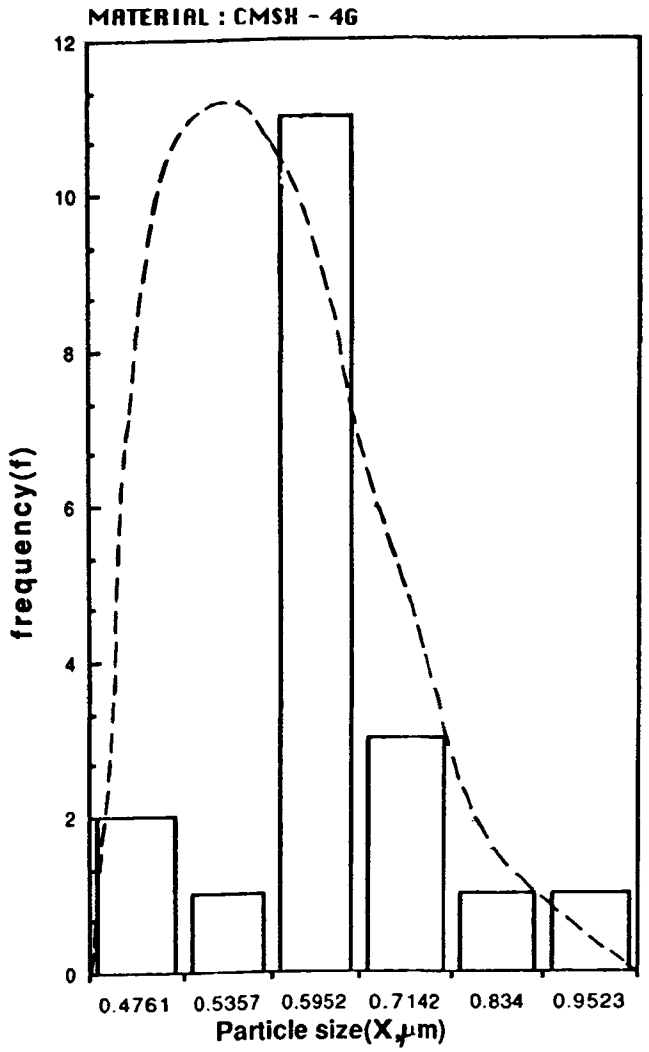

Fig. 6 Precipitate size distribution for heat treatment 2 (Table 2).

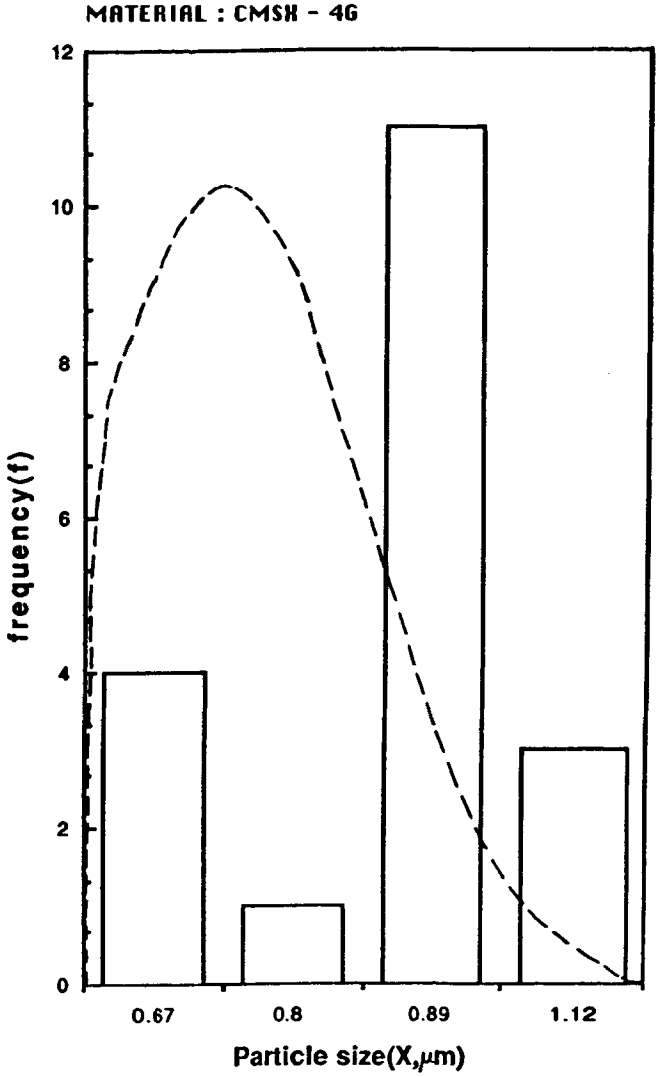

Fig. 7 Precipitate size distribution for heat treatment 3 (Table 2).

ume is approximately 320 kJ/mole. The activation energy for the coarsening of γ' in the nickel-aluminum binary system has been found to be 280 kJ/mole.[21] This value is approximately 15% lower than the value obtained in CMSX-4G (280 versus 320 kJ/mole). This higher activation energy in CMSX-4G obviously indicates that the coarsening rate of γ' will be lowered in the presence of rhenium. Thus, the addition of rhenium has resulted in a lower coarsening rate for γ'. The reason for the lower coarsening rate of γ' in this alloy in the presence of rhenium can be explained as follows. For the γ' precipitates to coarsen, rhenium has to diffuse away[13] from γ - γ' interface. Rhenium is a massive atom compared to nickel, therefore, the diffusion coefficient of rhenium is small. The diffusivity of nickel in a single crystal of nickel is on the order of 1.56×10^{-14} m^2/s at 1200 °C, whereas that of rhenium in nickel at the same temperature is 0.6×10^{-16} m^2/s. Rhenium also tends to increase the lattice parameter of γ.

Rhenium also introduces a negative misfit[20] between γ and γ'. This negative misfit results in a higher concentration of rhenium in the γ - γ' interface.[13] Hence, for the γ' particle to coarsen, rhenium must diffuse away from the interface. Since rhenium is a refractory element, its melting point is very high and, consequently, the diffusion coefficient of rhenium ($D_{\text{Re-Ni}}$) is significantly lower[13] than the self-diffusion coefficient of nickel. Hence, this lower diffusion coefficient ($D_{\text{Re-Ni}}$) has contributed to the lower coarsening rate of γ' in this alloy.

3.2 *Precipitate Size Distribution*

Precipitate size measurements were made from microstructures produced by aging at various temperatures for different times. The size distribution of the precipitate particles are plotted in Fig. 5 to 8 for various aging temperatures. The dashed line in these figures indicate the theoretical distribution predicted by the LSW theory for precipitate coarsening.

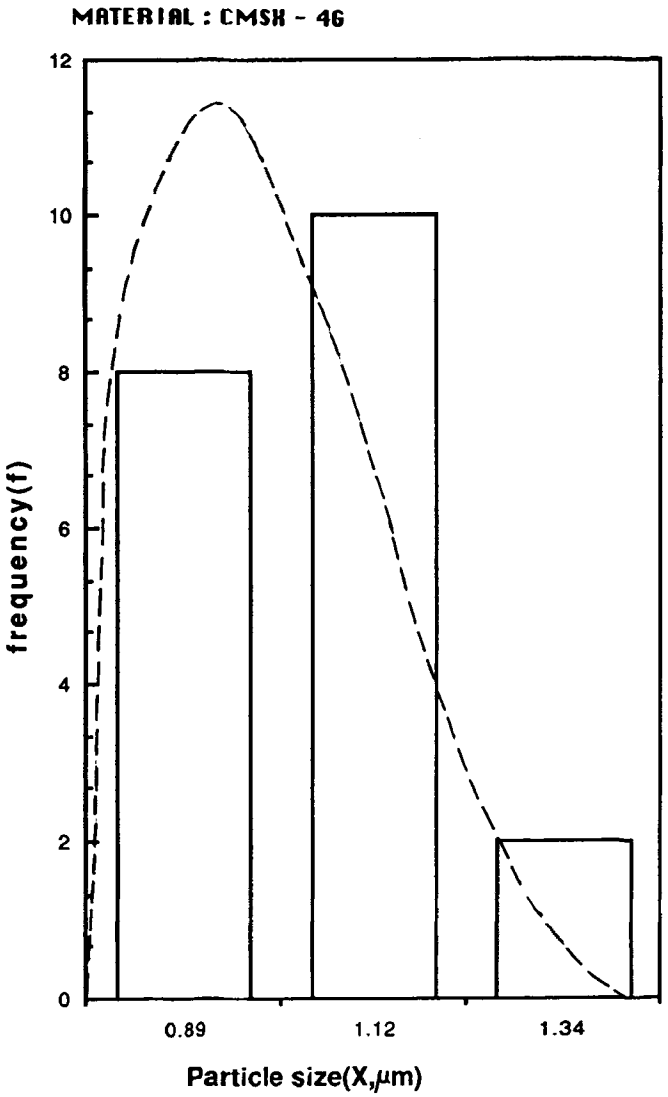

Fig. 8 Precipitate size distribution for heat treatment 4 (Table 2).

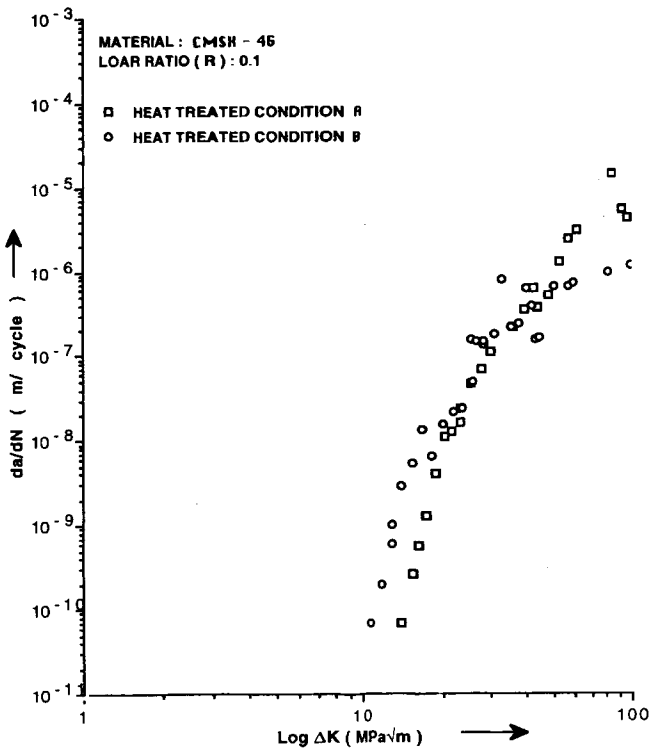

Fig. 9 Effect of γ' size on fatigue crack growth behavior of single-crystal nickel-base superalloy CMSX-4G at load ratio $R = 0.1$.

Table 4 Effect of Load Ratio on Fatigue Threshold

Material condition	Load ratio (R)	ΔK_{th}, MPa$\sqrt{m}$	Paris constants C	m
A	0.1	14.09	1.5^{-14}	4.6567
A	0.5	11.45	9.5^{-14}	3.9886
A	0.9	7.38	1.8^{-13}	4.8558
B	0.1	10.86	5.0^{-13}	3.7375
B	0.5	10.36	6.0^{-14}	4.4203
B	0.9	6.55	2.6^{-15}	6.3644

After a relatively short period of aging, there is a good correspondence between the shapes of the experimental distributions and those predicted by the LSW theory at each temperature. After longer aging times, the experimental distribution becomes broader than the theoretical distribution. Some earlier workers[17] also have observed similar deviations from the LSW theory after a longer aging period.

This deviation from the LSW theory for size distribution is apparently related to the large volume fraction of γ' precipitates observed in this alloy. Ardell[22] and Brailsford and Wynblatt[23] have shown that when the volume fraction of γ' precipitates was very large, such deviations from the theoretically predicted values are observed. Davies *et al.*,[22] on the other hand, pointed out that coalescence of the precipitates would have a similar effect on the observed distributions. Because both coalescence of precipitates as well as large volume function of γ' were observed in this alloy, it is very difficult to say which is the cause of the above deviations.

3.3 *Influence of γ' Precipitates on Fatigue Crack Growth Rate and Fatigue Threshold*

Figure 9 compares the fatigue crack growth behavior of material in heat treated conditions A and B at the same load ratio of $R = 0.10$. In Fig. 10 and 11, fatigue crack growth behavior of the materials in heat treated conditions A and B are compared at the same load ratios of $R = 0.5$ and 0.9, respectively. Table 4 reports the Paris constants C and m of the materials and fatigue threshold values of the materials at different load ratios. As reported in Table 4, the fatigue threshold values of this material are significantly higher than other single-crystal materials.[25]

It is also evident from these figures that fatigue crack growth rate is higher in heat treated condition B compared to heat treated condition A at same load ratios. Consequently, the fatigue threshold values are lower in heat treated condition B compared to heat treated A. Thus, it appears from the current test results that the smaller γ' precipitate size is beneficial as far

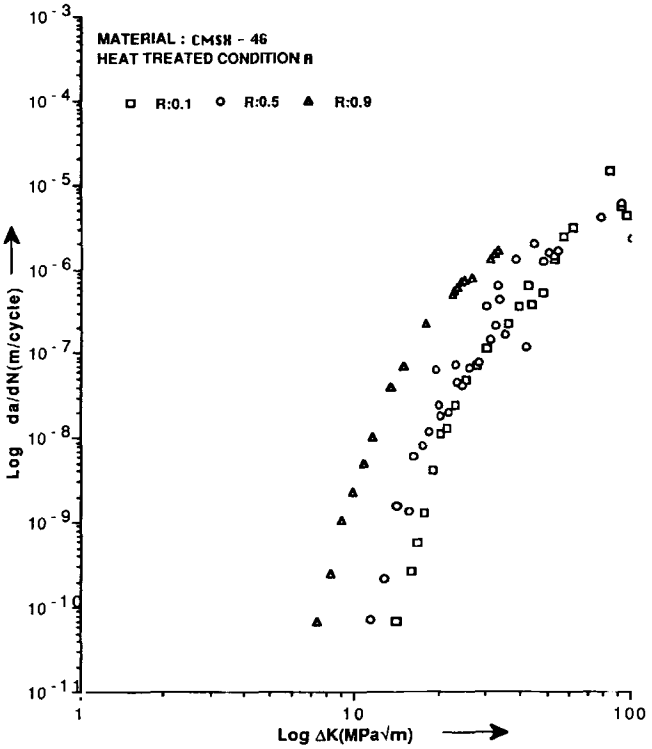

Fig. 15 Effect of load ratio (R) on fatigue crack growth rate in CMSX-4G, heat treated condition A.

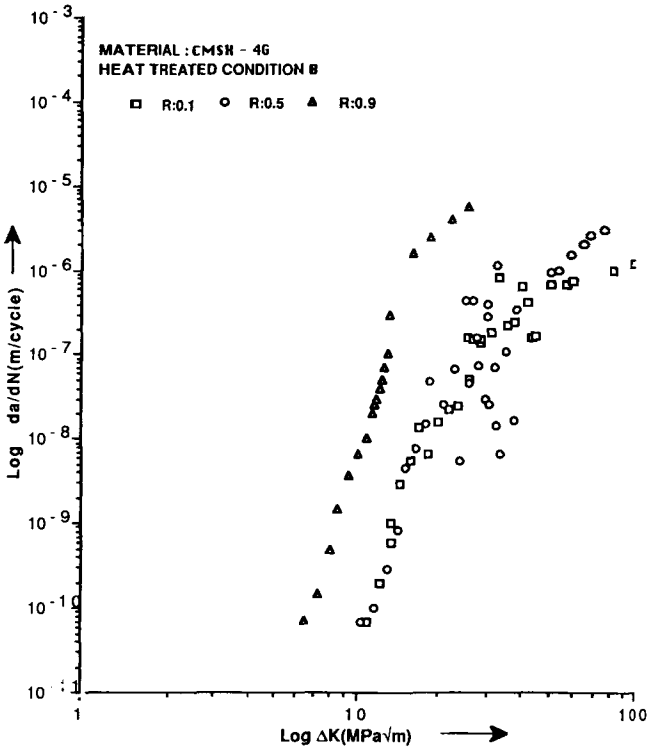

Fig. 16 Effect of load ratio (R) on fatigue crack growth rate in CMSX-4G, heat treated condition B.

results in a significantly higher value of fatigue threshold in CMSX-4G compared to other[30] single-crystal nickel-base superalloys.

The smaller γ' particles cause the crack to follow a more tortuous crack path in heat treated condition A material compared to heat treated condition B materials. Furthermore, extensive crack branching observed in threshold region caused a significant reduction in crack driving energy, which consequently leads to a higher value of fatigue threshold in heat treated condition A compared to heat treated condition B. The fractographs of the fast fracture regions are shown in Fig. 14(a) and (b), respectively. This region is characterized by dimples created by microvoid coalescence besides the presence of striations.

One interesting feature of this study is that, in the heat treated condition B material, the fatigue threshold values are similar at the load ratio of $R = 0.1$ and 0.5. This is related to the fact that the roughness-induced crack closures produced in this material are similar at these load ratios. Earlier workers[30] have also shown that a significant amount of roughness-induced crack closure can be produced in single-crystal nickel-base superalloys even at high load ratios such as $R = 0.5$.

The fatigue crack growth in single-crystal CMSX-4G was observed to occur along crystallographic planes of the type {111}. The crystallographic planes where the resolved shear stresses were maximum were the planes along which fracture occurred first. Cracking along {111} type planes continued throughout the crack growth process until final fracture occurred. Chan *et al.*[30] have also observed similar phenomenon in MAR-M200 single crystal.

3.4 *Influence of Load Ratio on Fatigue Crack Growth Rate*

Figures 15 and 16 report the effect of load ratio on fatigue crack growth behavior of the material in heat treated conditions A and B. It is obvious from Fig. 14 and 15 that fatigue crack growth rate increases with an increase in load ratio in heat treated conditions A and B, and consequently, fatigue threshold values decrease as the load ratio increases. This higher crack growth rate at higher load ratios can be explained on the basis of crack closure phenomena. At higher load ratios, the crack closure effect is significantly reduced and mechanical driving force for propagation of crack is higher. As a result of this, crack growth rate increase significantly with load ratios in both of these materials (heat treated conditions A and B).

Vosikovsky[31] analyzed the data from the literature concerning the effect of load ratio on fatigue threshold and have found that threshold decreases linearly with increase in load ratio. He proposed an empirical relationship of the nature $\Delta K_{th} = \Delta K_{tho}(1 - bR)$, where ΔK_{tho} is the value of threshold at load ratio $R = 0$ and b is a material-dependent constant. He also noted that both ΔK_{tho} and b increase with an increase in yield strength of the material. Barson[32] has also observed a similar linear relationship between fatigue threshold and load ratio. Klensil and Lucas[33] on the other hand observed a nonlinear power-law relation between threshold and load ratio, and they pro-

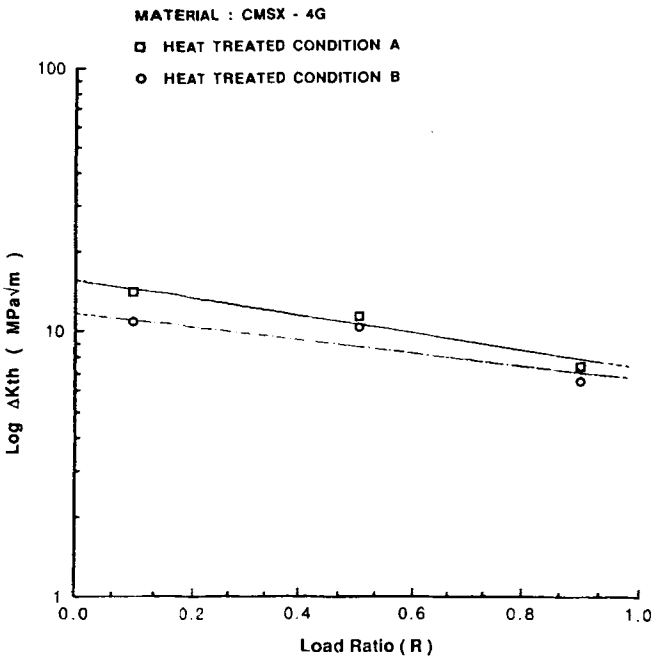

Fig. 17 Effect of load ratio (R) on fatigue threshold (ΔK_{th}).

posed a relationship of $\Delta K_{th} = \Delta K_{tho}(1 - R)^{\gamma}$, where γ is a constant whose value depends on the material.

The current test results show that none of the above models can accurately characterize the effect of load ratio on fatigue threshold in this material. Based on the above fact the data were analyzed with respect to a relationship developed earlier.[34] The developed model predicts a relationship between threshold and load ratio of the nature $\Delta K_{th} = (\Delta K_{tho})^{nmR}$, where n is the strain-hardening exponent of the material, m is a material constant, and R is the load ratio. Based on this equation, when the test results were plotted on a log-log scale in Fig. 17, a linear relationship was observed between log ΔK_{th} and R, which validates the above relationship.

4. Conclusions

The coarsening rate of γ' in single-crystal nickel-base superalloy CMSX-4G does not obey the cubic growth law. This deviation from the cubic growth law is apparently due to the presence of rhenium in this alloy and very large volume fractions of γ' in this alloy. The fatigue crack growth rate in CMSX-4G was found to increase with an increase in γ' precipitate size. Fatigue threshold values in single-crystal nickel-base superalloy CMSX-4G was observed to be higher in heat treated condition A compared to heat treated condition B at all load ratios in room-temperature ambient atmosphere. This indicates that the smaller γ' size is beneficial as far as the ΔK_{th} values are concerned.

Fatigue threshold values decrease with an increase in load ratios, and a previously developed model was found to be applicable to characterize the influence of load ratio on fatigue threshold in this material. Scanning electron fractographs show the presence of stage I type of crack growth, 45° to the tensile axis, in CMSX-4G. The crack path was mostly zigzag in this alloy. One interesting observation was that, in heat treated condition B material, ΔK_{th} values at $R = 0.1$ and 0.5 are almost similar. This is apparently due to the similarity in roughness-induced crack closure in these specimens, which may be introduced by out-of-plane secondary slip.

Acknowledgment

The authors are grateful to Cannon-Muskagon Corporation, Michigan, for supporting this work. Thanks are also due to Mr. Ken Harris of Cannon-Muskagon Corporation and Floyd Aberts of Ford Motor Company for their help during the various stages of this work. We are also grateful to Dr. Les Bartosiewicz and Mr. A.R. Krause for their help in the preparation of this manuscript. We are also thankful to Mr. David Nelson of the Word Processing Center at Wayne State University for carefully typing this manuscript.

References

1. M.J. Donachie, *Introduction to Superalloys: Superalloys Source Book*, American Society for Metals, 1984, p 3-25
2. D.R. Muzyka, *Special Technical Publication (STP) 672*, American Society for Testing and Materials, 1979, p 526-546
3. C.R. Brooks, *Heat Treatment, Structure and Properties of Non-Ferrous Alloys*, American Society for Metals, 1982, p 139-227
4. G.P. Sabol and R. Stickler, Microstructure of Nickel Based Superalloys, *Physica, Status Solidi*, Vol 35, 1969, p 11-22
5. C.T. Sims and W.C. Hagel, *The Superalloys*, John Wiley & Sons, 1972
6. Superalloys II, C.T. Sims, N.S. Stolloff, and W.C. Hagel, Ed., John Wiley & Sons, 1984, p 136-158
7. E.W. Ross and C.T. Sims, Nickel Based Alloys, in *Superalloys II*, C.T. Sims, N.S. Stolloff, and W.C. Hagel, Ed., John Wiley & Sons, 1984, p 97-132
8. R.G. Davies and N.S. Stolloff, *Trans. Metall. Soc. AIME*, Vol 233, 1965, p 714-718
9. M. Gell, D.N. Duhl, and A.F. Giamei, The Development of Single Crystal Superalloy Turbine Blades, *Superalloys Source Book*, American Society for Metals, 1984, p 297-332
10. G.R. Leverant and B.H. Kear, *Metall. Trans.*, Vol 1, 1970, p 491-498
11. G.S. Hoppin and W.P. Danesi, *Superalloys II*, John Wiley & Sons, 1984, p 549-560
12. Tech. Rep. Advanced Mater. Proc., July 1991
13. A.F. Giamei and D.L. Anton, Rhenium Additions to a Nickel Based Superalloy: Effects on Microstructure, *Metall. Trans. A*, Vol 16, Nov, 1985, p 1997-2005
14. Annual Book of ASTM Standards, ASTM E-647, Vol 03.01, 1991, p 642-657
15. R.A. Ricks, A.J. Porter, and R.C. Ecole, *Acta Metall.*, Vol 31, 1983, p 43-46
16. I.M. Lifshitz and V.V. Slyozov, *J. Phys. Chem. Solids*, Vol 19, 1961, p 35-64
17. C. Wagner, *Z. Elektrochem*, Vol 65, 1961, p 581-583
18. A.A. Hopgood and J.W. Martin, *Mater. Sci. Technol.*, Vol 2, June 1986, p 543-556
19. A.J. Ardell, *Acta Metall.*, Vol 20, 1983, p 61-66

20. D. McLean, *Met. Sci.*, Vol 18, 1984, p 249-260
21. R.W. Swalin and A. Martin, *Transactions of AIME,* May 1956, p 567-572
22. A.J. Ardell, R.B. Nicholson, and J.D. Eshelby, *Acta Metall.*, Vol 14, 1966, p 1295-1308
23. A.D. Brailsford and P. Wynblatt, *Acta Metall.*, Vol 27, 1979, p 489-494
24. C.K.L. Davies, P. Nash, and R. Stevens, *Acta Metall.*, Vol 28, 1980, p 179-186
25. J.S. Crompton and J.W. Martin, *Metall. Trans. A*, Vol 15, Sept 1984, p 1711-1719
26. S.D. Antolovich and J.E. Campbell, Fracture Properties of Superalloys, *Superalloys Source Book*, American Society for Metals, 1984, p 112-136
27. H.F. Merrick and S. Floreen, *Metall. Trans. A*, Vol 9 (No. 2), Feb 1987, p 231-233
28. J. Bartos and S.D. Antolovich, *Fracture 1977*, Vol 2, 1977, p 996-1006
29. W. Elber, *Eng. Fract. Mechan.*, Vol 21, 1970, p 323-370
30. K.S. Chan, J.E. Hack, and G.R. Leverant, *Metall. Trans.*, Vol 18, Apr 1987, p 581-592
31. O. Vosikovosky, *Eng. Fract. Mechan.*, Vol 11, 1972, p 595-602
32. J.M. Barson, *W.R.C. Bull.*, Vol 194, May 1974, p 123-136
33. M. Klensil and P. Lucas, *Mater. Sci. Eng.*, Vol 9, 1972, p 231-236
34. S.K. Putatunda, *Trans. Ind. Inst. Metals*, Vol 42 (No. 2), 1990, p 135-142